Properties of Asymmetric Polyimide Ultrafiltration Membranes. I. Pore Size and Morphology Characterization*

MOHAMMAD N. SARBOLOUKI, *Energy and Materials Research Section, Jet Propulsion Laboratory, California Institute of Technology, Pasadena, California 91103*

Synopsis

Properties of asymmetric UF membranes made by solution casting of aromatic polyimides as a function of fabrication conditions are reported. The characteristic properties investigated include: the overall porosity, hydraulic permeability, the equivalent pore size of the skin layer (via a newly developed general diagram), and morphological features shown by the scanning electron microscope. It was found that as casting solution concentration and/or evaporation period was increased, the average pore size decreased while the skin thickness increased. At low casting solution concentrations the membranes were highly porous and the precipitated polymer phase had a granular structure consisting of aggregates of precipitated polymer micelles. While at high concentrations marcrovoid porosity was reduced but the precipitated polymer phase had a spongy structure. The interstitial openings of the granular skin structure of a membrane made from 15% polymer solution with no evaporation as revealed by SEM showed pore size values that were close to those calculated through pore models.

INTRODUCTION

Ultrafiltration (UF) membranes have been made from numerous materials such as cellulose derivatives, acrylics, polysulfones, polycarbonate, fluoropolymers, polyamides, and inorganic substrates. Currently available commercial UF membranes made of organic polymers are limited to operating temperatures of 50–60°C, but even at these temperatures their lifetimes are often too short. There are some applications that demand higher operating temperatures, including, for example, water reuse under sterilizing conditions in space, or recycling of hot process waters in various industries. In our search for UF membranes with high temperature capability we have prepared and characterized membranes prepared from soluble polyimides. This first report presents part of our findings regarding their fundamental characteristics. Their UF performance at high temperatures will be the subject of a subsequent report.

PROPERTIES OF THE POLYIMIDE

The polyimides used was Upjohn's PI-2080 and Ciba-Geigy's XU-218. The former is made by polycondensation of benzophenone tetracarboxylic acid and

* This article presents the results of one phase of research carried out at the Jet Propulsion Laboratory, California Institute of Technology, under Contract No. NAS7-100 sponsored by the National Aeronautics and Space Administration.

Journal of Applied Polymer Science, Vol. 29, 743–753 (1984)
 CCC 0021-8995/84/030743-11$04.00

a mixture of diisocyanates [toluene diisocyanate plus methylene bis(phenyl isocyanate)][1] while the latter is made from the reaction between 5(6)-amino-1-(4′-aminophenyl)-1,3,3-trimethylindane (DAPI) and benzophenonetetracarboxylic dianhydric:

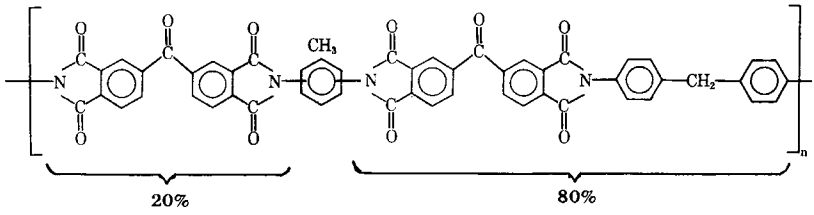

PI-2080

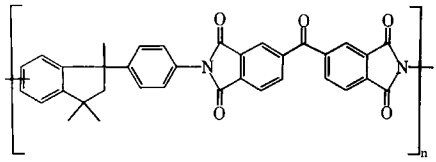

XU-218

These polymers are soluble in solvents like *N*,*N*-dimethylacetamide, *N*,*N*-dimethyl-formamide, *N*-methylpyrrolidone, and dimethylsulfoxide which render it solution castable. The polymers are recommended for high temperature applications. Table I summarizes some of their physical properties of interest.

TABLE I
Physical Properties of the Polyimide Used in Membrane Fabrication

		XU-218[2]	PI-2080[3]
Glass transition temp (°C)		320–330	310–315
Heat deflection temp (°C)			270–280
Oxygen index			44%
Linear coeff. therm. expansion ($°C^{-1}$)		5×10^{-5}	5.9×10^{-5}
Specific gravity		1.2	1.4
Tensile strength @ 25°C (Pa)		8.7×10^{9}	1.2×10^{8}
@ 285°C	3×10^{7}		2.9×10^{7}
Tensile modulus @ 25°C		2.9×10^{9}	1.3×10^{9}
@ 285°C			6.6×10^{8}
Elongation at break @ 25°C		48.6%	10%
Flexural strength @ 25°C (Pa)			2×10^{8}
@ 285°C			3.4×10^{7}
Flexural modulus @ 25°C			3.3×10^{9}
@ 285°C			1.1×10^{9}
Compressive strength @ 25°C (Pa)			2×10^{8}
Compressive modulus @ 25°C (Pa)			2×10^{9}
Compression creep per day @ 1.87 GPa, @ 25°C			0.04%
@ 312°C			0.47%

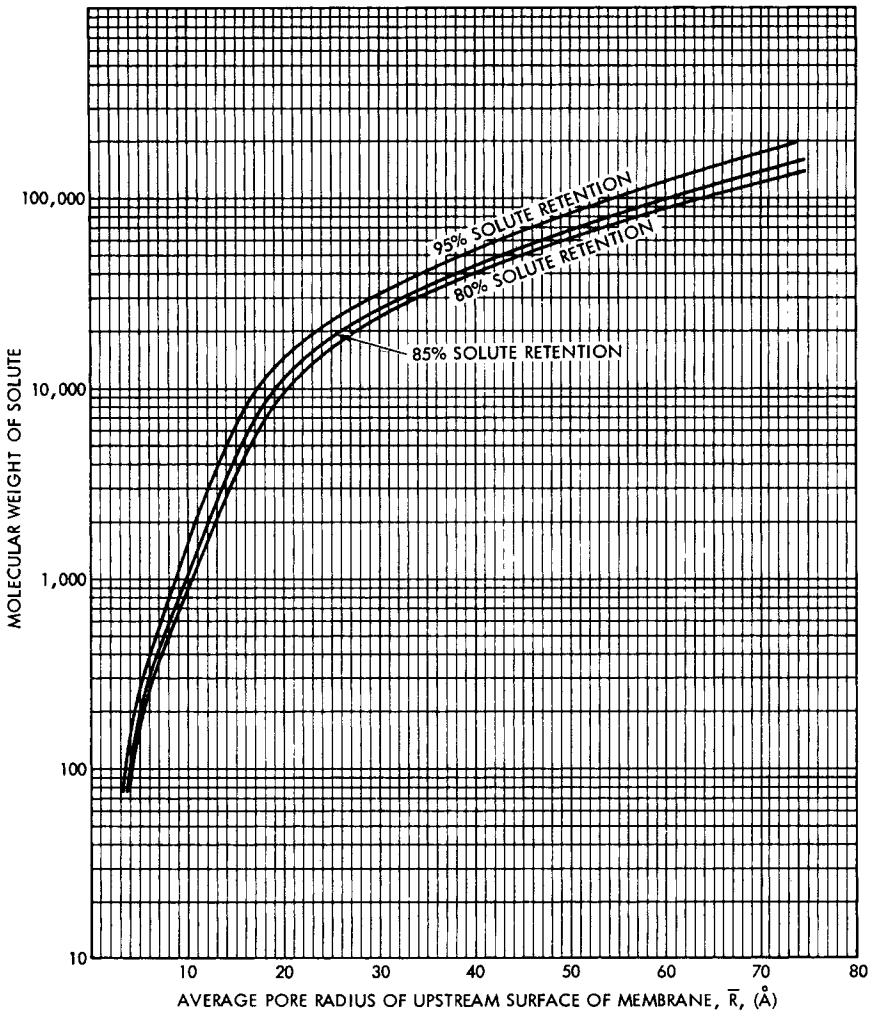

Fig. 1. General correlation between solute molecular weight and the average pore radius of the upstream surface of the membrane at 80%, 85%, and 95% solute retention. For details see the Appendix.

There seems to be only one type of polyimide membrane reported in the literature, and that involves insoluble polyimides which are prepared from polycondensation of the cast precursor in a process which is both tedious and costly.[4] Therefore, it was of interest to exploit the unique features of the soluble polyimides (PI-2080 and XU-218) in obtaining asymmetric UF membranes.

EXPERIMENTAL

Skin type asymmetric membranes were prepared from polymer solutions in DMAc following the conventional solution casting and phase inversion technique originated by Loeb and Sourirajan.[5] After their formation membrane thicknesses were measured with a thickness gage; their water content determined by

TABLE II
Properties of UF Membranes Obtained from PI-2080 as a Function of Casting Conditions

Property investigated	Polymer concentration (%) in DMAc								
	15			20			25		
	Evap. time (min)			Evap. time (min)			Evap. time (min)		
	0	7	15	0	7	15	0	7	15
Water content %	82	79	75	77	72	68	73	70	65
Overall porosity[a]	0.86	0.84	0.80	0.82	0.79	0.75	0.79	0.77	0.73
Hydraulic permeability (cm/s dyne × 10^8)	5.2	0.69	0.29	1.5	0.36	0.16	0.44	0.21	0.1
Pore size (Å)	120	105	50	94	77	40	68	56	30

[a] Overall porosity is defined as volume of water in the membrane divided by the total volume of the membrane.

weighing wet and vacuum dried specimens. Hydraulic permeabilities were measured from the slope of pure water flux vs. applied pressure. The equivalent (average) pore sizes of the membrane skins were estimated from studying the solute retention of the membranes against dextran fractions (molecular weight 10,000–250,000) and the use of pore (sieve) models as described below. Scanning electron photomicrographs of membrane cross sections were obtained to study the effects of fabrication conditions on their morphology and to determine

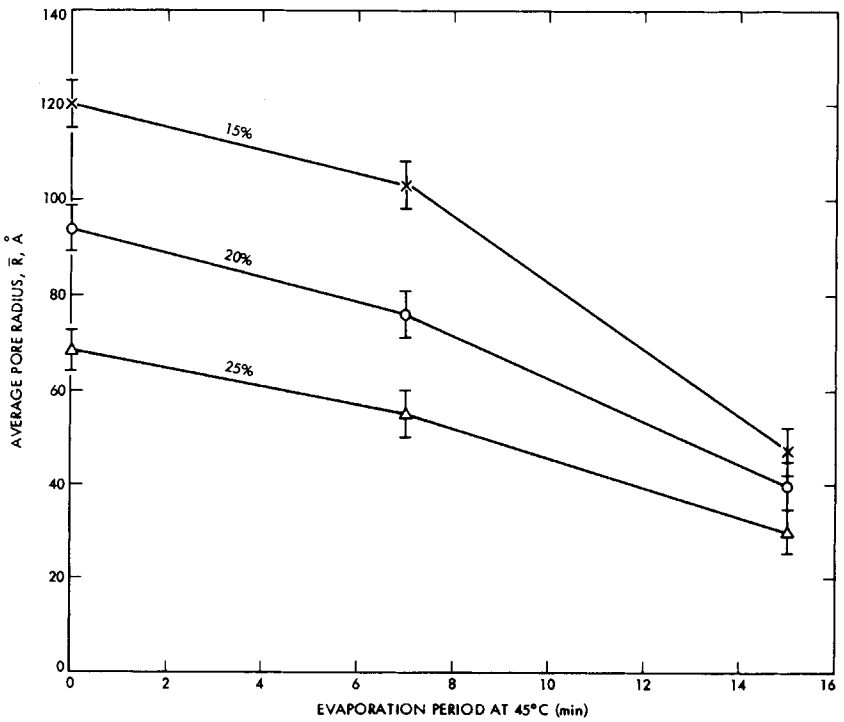

Fig. 2. Dependence of equivalent pore size [determined from pore model described by Fig. (1)] and evaporation period for membranes prepared from casting solutions ranging from 15% to 25% (wt) in concentration.

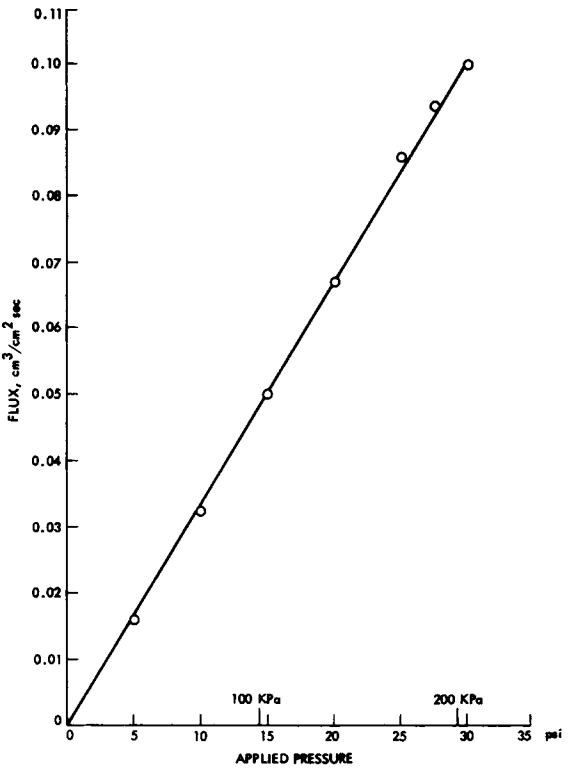

Fig. 3. Representative of the relation between pure water flux and applied pressure, in this case a polyimide membrane made from 15% polymer solution without evaporation.

whether skin pores could be seen and if there was a correlation with calculated pore sizes.

PORE SIZE CHARACTERIZATION

There are essentially two general categories of pore models used in membrane characterization: (a) sieve models[6] and (b) pore flow models.[7] The former apply to electrically neutral porous membranes (whether homogeneous or not) and yield an equivalent pore size characteristic of only the structure of the upstream layer of the membrane (when tested in UF mode).[8] The latter models, which combine tracer diffusivity, hydraulic permeability, and porosity in obtaining the equivalent pore sizes, are applicable only to homogeneous membranes (whether porous or not).[6] Thus, in dealing with the asymmetric UF membranes the former models are applicable, and the equivalent pore sizes obtained characterize their skin structure. Two classes of sieve models may be considered: (i) ideal sieves which consider only the exclusion effects at the pore entrance during UF and (ii) those that consider a combination of entrance sieving and frictional effect within the pore. For reasons described in the Appendix only simple sieve models are applicable for the description of the steady state UF.

To determine the equivalent pore size of the membrane, the experimentally measured solute retention, SR %, of the membrane against a solute of known size,

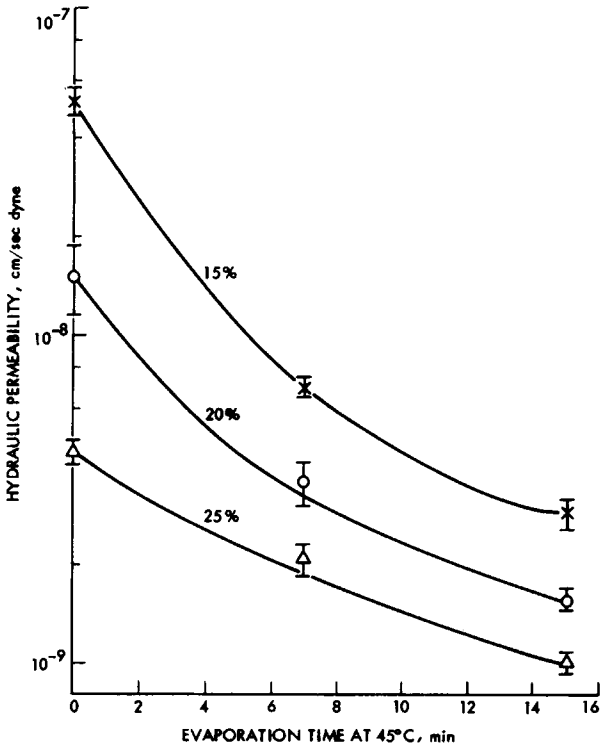

Fig. 4. Relation between hydraulic permeability and evaporation period for membranes prepared from casting solutions ranging from 15% to 25% (wt) in concentration.

$\bar{a}$, is used to read off the corresponding $\bar{R}$ from any of the three curves in Figure 1.

RESULTS AND DISCUSSION

Table II and Figures 2–4 show some of the representative properties as a function of fabrication conditions. SEM photomicrographs of membranes prepared from various casting solutions are shown in Figures 5–8.

The hydraulic permeability data reflect the fact that when casting solution concentration and/or evaporation period increases, the membrane resistance also increases. The decrease in equivalent pore size as a function of concentration and evaporation time (Fig. 2), demonstrates the contribution of pore size in decreasing the hydraulic permeability. Other contributors are the reduction in overall membrane porosity, and increases in skin thickness and density as evidenced by SEM.

The SEM photomicrographs reveal a substantial amount of information regarding the structure of various membranes and mechanisms underlying their morphogenesis. At low polymer concentrations (Fig. 5 and 6), the membranes have a highly open structure with many fingerlike cavities and macrovoids. The membrane matrices consist of granular aggregates of precipitated polymer miceles, which prevail even in the skin regions [Figs. 5(a), 5(b), 5(c), 6(a), and 6(b).

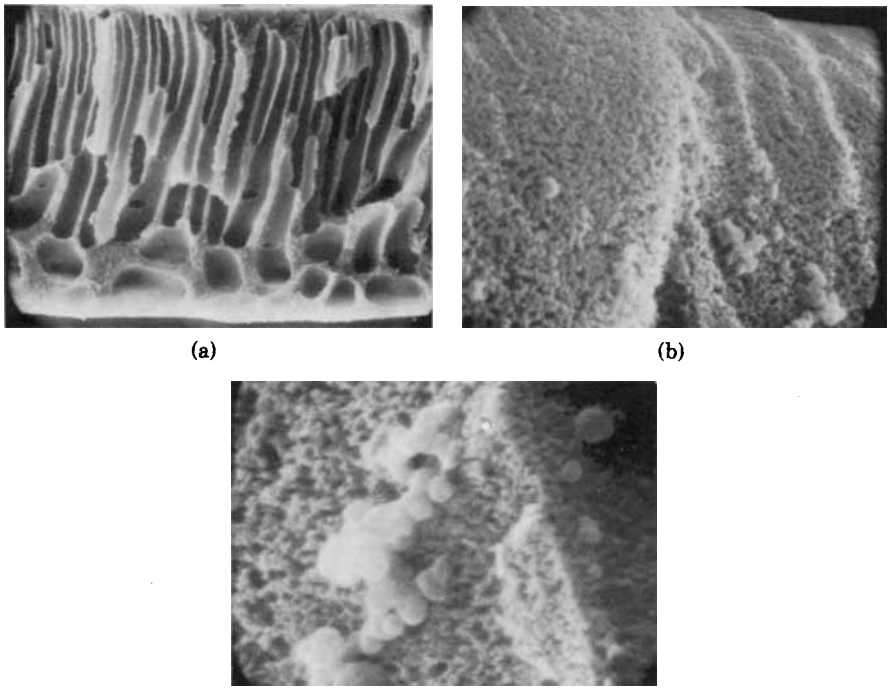

(a) (b)

(c)

Fig. 5. SEM photomicrographs of a polyimide membrane made from 12.5% polymer solution without evaporation: (a) overall cross section @ 450 ×; (b) a view of skin edge @ 2000 ×; (c) a portion of (b) @ 20,000 ×.

The skin structure itself has a graded pore structure, tending to decrease as one moves towards the skin surface [Figs. 6(c), 7(b), and 8(b)].

In the case of the membrane cast from a 15% polymer solution with no evaporation, the view of the skin surface, as shown by Figure 5(b), reveals a granular structure with interstitial spaces of the order of 200–700 Å which correspond to radii in the range of 100–350 Å. Unfortunately, greater resolutions could not be achieved with this SEM. The calculated equivalent pore size for this membrane, as shown in Figure 8, is 110–125 Å, which is in reasonable agreement with SEM results considering the subleties involved such as: (a) inadvertant changes in skin structure during SEM specimen preparation and low resolution of the SEM; (b) idealities assumed in the derivation of pore models, e.g., rigid spherical solute, monodisperse pores, nonadsorptivity of solute by the membranes, absence of boundary layer effects; and (c) assumptions involved in derivation of the radius of gyration, e.g., a monodisperse linear polymer and neglecting concentration effects.

Regarding the overall cross-section morphology of the various membranes, the commonly accepted mechanism for formation of phase inversion membranes seems appropriate. The principal tenets of this mechanism are that three parameters control membrane morphogenesis: (1) rate of solvent departure from cast polymer solution, (2) rate of nonsolvent flow into the polymer solution, and (3) concentration of polymer at the point of precipitation.[9–11] Thus, when the

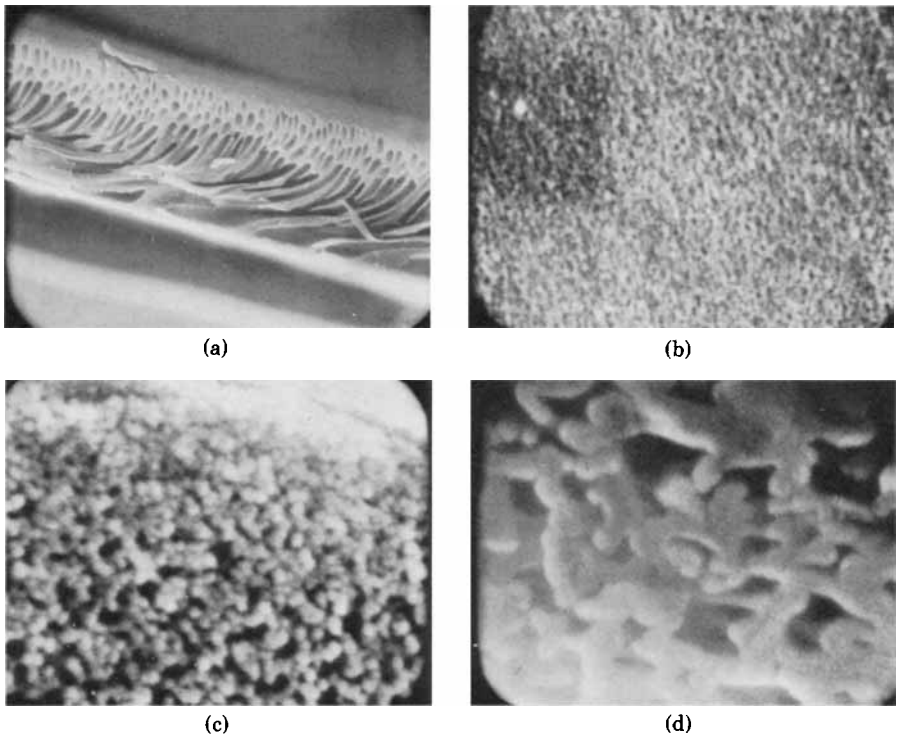

Fig. 6. SEM photomicrographs of polyimide membrane made from 15% solution without evaporation: (a) overall cross section @ 270 ×; (b) skin surface @ 30,000 ×; (c) a view of skin edge @ 30,000 ×; (d) a view of bottom layer edge @ 30,000 ×.

cast film of polymer solution is immersed in nonsolvent (water), there is an immediate departure of solvent from the surface of the polymer solution into the water, while simultaneously there is an inflow of water into the polymer solution. This exchange of solvent/nonsolvent across the fresh interface takes place almost instantly and leads to a rapid polymer precipitation at the interface, thereby producing the dense and thin skin. The reason for denseness is that the system enters the miscibility gap so quickly that there is not time for liquid/liquid phase separation. The polymer solution simply loses almost all of its solvent, and one might say it literally dries out instantly. (Of course, it will contain some residual solvent and some adsorbed nonsolvent.) In the case of dilute polymer solutions (Figs. 5 and 6) the precipitated polymer phase in the skin layer seems to exist in the form of granular aggregates which reflect the fact that initial steps in precipitation involve some form of micellization or formation of vesicles consisting of a spherical skin enclosing the remainder of the polymer solution. Such a process seems reasonable in light of the fact that low viscosity, and surface tension forces favor micellization. Initially these micelles or vesicles contain some residual solvent and are deformable under the forceful flow of solvent from the unprecipitated sublayer. They are fused together at their contact points leading to the formation of granular aggregates of subsequently solid micelles.

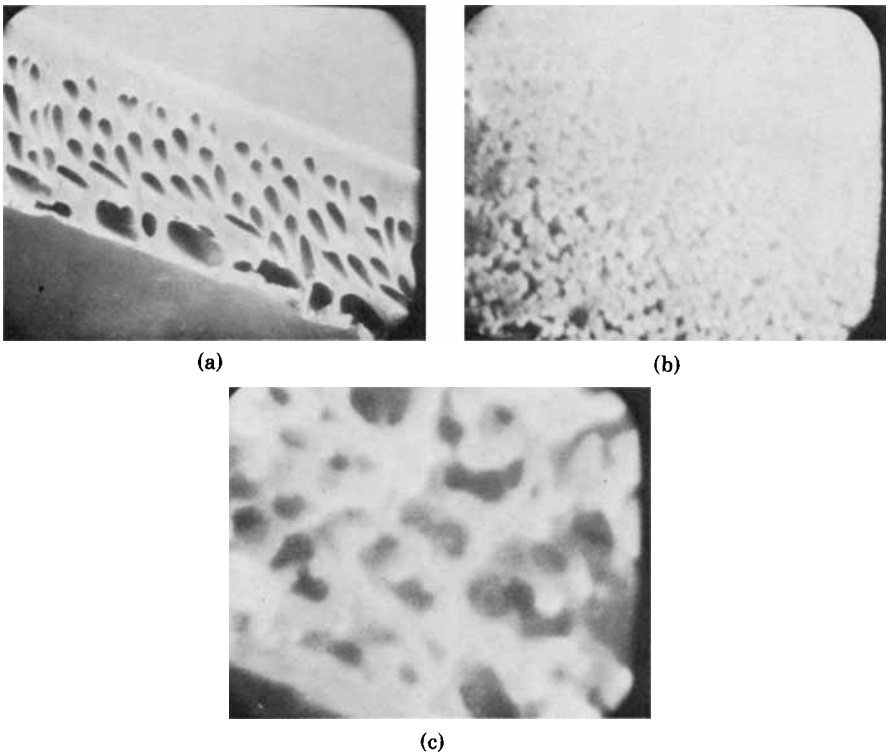

Fig. 7. SEM photomicrographs of polyimide membrane made from 20% solution without evaporation: (a) overall cross section @ 300 ×; (b) skin edge @ 30,000 ×; (c) bottom edge @ 30,000 ×.

Once the skin is formed, it becomes the rate determining barrier to the exchange of solvent/nonsolvent and the precipitation of the sublayer proceeds at a slower speed. Another consequence of skin formation is fixation of the volume of cast film, thereby limiting its volumetric changes. Under these circumstances and sublayer polymer solution experiences a different mode of precipitation. Since solvent/nonsolvent exchange takes place at a slower pace, there is ample opportunity for phase separation whereby domains of a polymer-rich phase (containing some solvent and slight amount of nonsolvent) are in a quasiequilibrium existence with liquid domains of a solvent-rich phase (containing most of the penetrated nonsolvent). Eventually when the solvent-rich domains have been replaced by nonsolvent and the residual solvent has departed from the polymer rich domains, the membrane morphology is established. The spaces occupied by the solvent rich domains become voids and macrovoids as seen by SEM. Since dilute polymer solutions contain more solvent, they produce greater amounts of large macrovoids, whereas more concentrated solutions produce less of them.

Another difference between the morphology of membranes produced from dilute and concentrated polymer solutions is the structure of the precipitated polymer forming their matrices [Figs. 7(c), 8(c), and 8(d)]. Dilute polymer solutions produce granular aggregates while concentrated solutions yield a continuous spongy structure. This is due to higher viscosity and surface tension

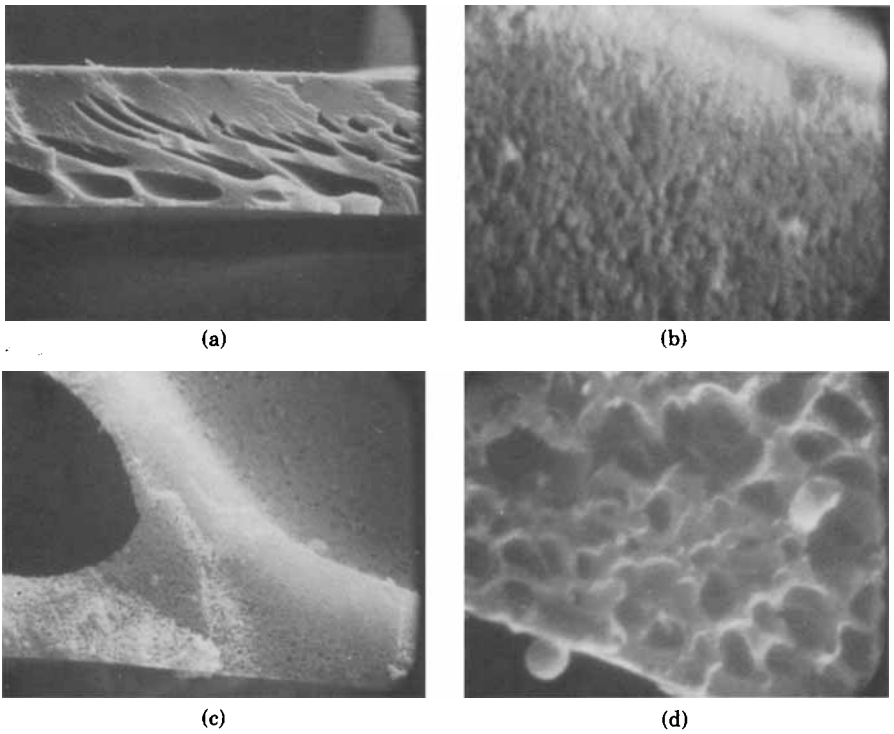

Fig. 8. SEM photomicrographs of polyimide membrane made from 25% solution without evaporation: (a) overall cross section @ 200 ×; (b) skin edge @ 30,000 ×; (c) bottom edge @ 2000 ×; (d) a portion of (c) @ 30,000 ×.

of concentrate solutions which prevent micellization at the onset of phase separation. Interestingly enough, however, the skin structure of membranes produced from concentrated polymer solutions [Figs. 7(b) and 8(b)], although thicker and denser, still look granular. This is probably due to rapid precipitation of the skin layer which, as mentioned, prevents liquid/liquid phase separation.

APPENDIX: PROPOSED METHOD OF ESTIMATING THE MEMBRANE PORE SIZE

Viewing the UF and RO membranes as sieves, in order to develop the relationship between the molecular weight cutoff and membrane pore size, it is first necessary to find a way of translating the

TABLE III
A Comparison of the Average Pore Radii, $\bar{R}$, Obtained from Figure 1 with Those of the Literature and Manufacturer

Amicon Membrane							
Identification code	UM05	UM2	YM5	UM10	PM10	XM50	XM100
Mfr.'s reported SR %	90	80	90	90	65	80–100	80–100
@ given mw	594	594	10,000	10,000	10,000	50,000	100,000
$\bar{R}$, by our method (Å)	9.3	12.7	16.3	18.2	21.8	37–46	53–63
$\bar{R}$, from literature (Å)	—	—	—	7–15[13]	10–20[13]	30–73[14]	68–76[14]
$\bar{R}$, from mfr. (Å)	10.5	12	—	15	19	33	55

solute molecular weight into a corresponding molecular size and from the latter estimate the pore size via a valid mathematical model. Details of this procedure are reported elsewhere.[12]

In brief, the first, step was accomplished by plotting the solute size (Stokes' radius or radius of gyration) as a function of molecular weight. Then using a slit sieve model the solute retention was related to the solute size and the pore size, i.e.,

$$SR\% = 100(\bar{a}/\bar{R}) \tag{1}$$

where $\bar{a}$ = solute radius and $\bar{R}$ = pore radius (meaning half- width of the slit). Combining the general curve relating solute molecular weight to radius and the above equation, a series of diagrams were generated, some of which are shown in Figure 1. With the aid of this diagram, one can directly read off the average pore size of the membrane once an inert solute has been found whose SR % is between 80% and 100%, i.e., once its molecular weight cutoff has been determined. For example, if an UF membrane exhibits a solute retention of 95% against 70,000 molecular weight dextran (at steady state in a well-stirred system), its average pore radius (upstream) is read as 46 Å.

To verify the validity of the above diagram, the available data (molecular weight cutoff) on commercial membranes were used to read off their corresponding average pore radii. The results are shown in Table III where they are compared with the manufacturers reported pore sizes as well as with those reported in the literature based on electron microscope examination[13] and flow measurement techniques.[14] It is seen that the estimated pore sizes from Figure 1 are in surprisingly good agreement with others considering the assumption made in the derivation of the pore model such as monodisperse rigid solute molecule and monodisperse pores as well as manufacturing variations and handling complications.

References

1. L. M. Alberinos, W. J. Farrisey, and J. S. Rose, U.S. Pat. 3,708,458 (1973).
2. J. H. Bateman, W. Geresy, and D. S. Neiditch, *Preprints Organic Coatings Plastics, Am. Chem. Soc.*, **35,** 77 (1975).
3. K. W. Rausch, W. J. Farrisey, and A. A. Sayiegh, *Proceedings of the 28th Annual Tech. Conference of Soc. Plast. Ind., Sect. 11-E*, 1973, p. 1.
4. H. Strathmann, *Desalination*, **26,** 85 (1978).
5. S. Loeb and S. Sourirajan, *Adv. Chem. Ser.*, **38,** 117 (1962).
6. M. N. Sarbolouki, *Ion Exchange Membranes*, **2,** 117 (1975).
7. M. N. Sarbolouki, I. F. Miller, *Desalination*, **12,** 343 (1973).
8. M. N. Sarbolouki, *J. Polym. Sci. Part C, Polym. Lett.*, **15,** 169 (1977).
9. M. A. Frommer, I. Feiner, O. Kedem, and R. Bloch, *Desalination*, **7,** 393 (1970).
10. M. N. Sarbolouki, *J. Polym. Sci., Part C, Polym. Lett.*, **11,** 763 (1973).
11. H. Strathmann, K. Kock, P. Amar, and R. W. Baker, *Desalination*, **16,** 179 (1975).
12. M. N. Sarbolouki, *Separation Sci. Tech.*, **17,** 381 (1982).
13. R. W. Baker, F. R. Eirich, and H. Strathmann, *J. Phys. Chem.*, **76,** 238 (1972).
14. J. H. Preusser, *Kolloid Z. Z. Polym.*, **250,** 133 (1972).

Received October 21, 1980
Accepted June 29, 1981
Corrected proofs received November 3, 1983